Grain Structures in Aluminum Alloy GTA Welds

T. GANAHA, B. P. PEARCE, AND H. W. KERR

The grain structures in two dimensional GTA welds of a number of commercial aluminum alloys have been studied in order to clarify the mechanisms of grain refinement in welds. At low welding speeds and heat inputs the structures were either axial (continuous grains along the weld centerline) or stray (intermittent new grains). At higher speeds and heat inputs the structures were generally either columnar to the weld centerline, or contained some equiaxed grains at the center. Regression analyses indicated that both stray grains and equiaxed grains were favored by increased titanium content. In several alloys, titanium-rich compounds, and in one alloy, zirconium-rich compounds were found at the centers of dendrites. It is concluded that both stray and equiaxed grains originate by heterogeneous nucleation, with possible secondary effects due to constitutional undercooling.

THE properties of a weld are related to its grain structure. For example, welds in which the grains grow straight to meet at a distinct centerline are more likely to exhibit hot cracking than welds in which grains gradually curve to follow the heat flow.[1] Grain refinement also reduces the sensitivity to hot cracking.[2,3] Such factors have led to the investigation of grain structures in GTA welds in several materials.

In aluminum alloys, unlike steel welds,[4] the solidification structure is readily revealed, and a variety of structures have been observed by Japanese workers.[5,6] Their explanations for various structural transitions are based mainly on the changes in growth rate and temperature gradient, with different welding conditions, affecting the amount of constitutional undercooling at the advancing solid-liquid interface. For example, the transition to an equiaxed structure was ascribed to a sufficiently long constitutionally undercooled zone.[5,6]

Both theory and experiment have shown that solidification morphology in any given alloy depends on the ratio of G/R where R is the solidification velocity and G the temperature gradient normal to the macroscopic interface. For different alloys the critical ratio of G/R (or $G/R^{1/2}$) depends mainly on the freezing range.[1] Hence if constitutional undercooling is determining the transition to equiaxed grains, the critical G/R ratio should increase as the freezing range of the alloy increases. Using the reported[6] length of the constitutionally supercooled zone to calculate the temperature gradient along the weld centerline G_c, and the reported structural transition to determine the critical solidification velocity (taken as the welding speed V at the chosen[6] heat input of 1400 J/s) the ratio of G_c/V for the transition to equiaxed grains may be calculated. Figure 1 shows the calculated G_c/V *vs* the freezing range. Contrary to solidification theory, no correlation between the two is apparent. This is inconsistent with the proposal that the transition to equiaxed grains is dependent on the degree of constitutional undercooling.

The above analysis, as well as the original analyses[5,6] may be criticized on the basis that the temperature gradients and solidification velocities are those along the weld centerline, whereas the equiaxed transition may take place closer to the fusion line. More accurate calculations of G and R are available[7] which could be used to refine the calculations, but other grain refinement mechanisms should also be considered. In ingots, other observed mechanisms include dendrite arms breaking off via fluid flow or remelting, nucleation at the surface, and bulk heterogeneous nucleation.[3,4] A more detailed metallographic study on a wider range of alloys was carried out to examine the structural transitions, in particular the formation of equiaxed grains, more closely.

EXPERIMENTAL METHODS AND MATERIALS

The alloys studied are listed in Table I. The specimens employed were 50 mm wide, 125 mm long and 1.5 mm thick. Direct current GTA welding, with

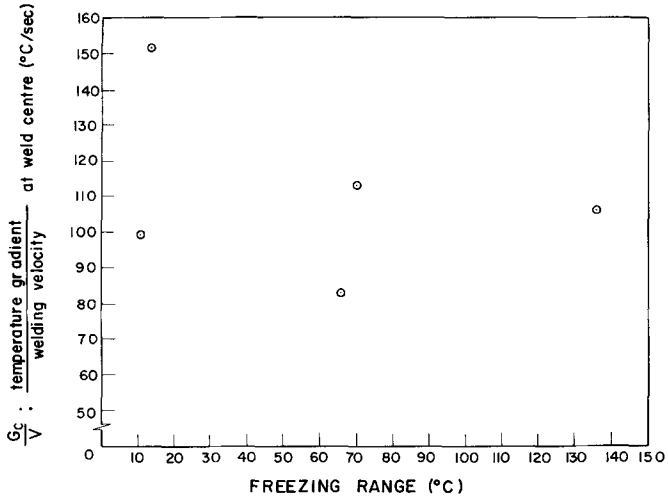

Fig. 1—The ratio Gc/V (temperature gradient at the weld centerline over welding speed) for the welding conditions giving equiaxed grain formation, using a heat input 1400 J/s, *vs* reported freezing range, according to Ref. (6).

T. GANAHA, formerly Graduate Student, University of Waterloo, is now Welding Engineer, Guelph Engineering Co. Ltd., Guelph, Ontario, Canada. B. P. PEARCE and H. W. KERR are Research Assistant and Professor, respectively, Department of Mechanical Engineering, University of Waterloo, Waterloo, Ontario, Canada.

Manuscript submitted December 27, 1979.

ISSN 0360-2133/80/0811-1351$00.75/0

Table I: Chemical Analysis of Aluminum Alloys

	Element (wt pct)									
Alloy	Cu	Si	Fe	Mg	Mn	Zn	Ti	Cr	Zr	Al
1100	0.06	0.13	0.55	0.002	0.008	0.004	0.02	0.001	NA	Bal
3003	0.10	0.17	0.63	0.02	1.08	0.04	0.013	NA	NA	Bal
5052	0.018	0.08	0.24	2.28	0.028	0.017	0.013	0.18	0.001	Bal
5083	0.02	0.16	0.30	4.18	0.75	0.02	0.024	0.06	NA	Bal
5454	0.04	0.10	0.25	2.58	0.76	0.06	0.005	0.10	NA	Bal
6061	0.31	0.62	0.32	0.90	0.005	0.006	0.02	0.17	NA	Bal
7004	0.03	0.17	0.23	1.55	0.49	4.45	0.020	NA	0.13	Bal

N/A = Not Analyzed

electrode positive, was used to produce "bead-on-plate" welds which completely penetrated the sheets and gave essentially parallel fusion boundaries. All welds were made using argon shielding gas, a 4.75 mm tungsten-2 pct thoria electrode with a hemispherical tip, and an arc gap of 2.4 mm. The low density and high surface tension of aluminum permitted a range of heat inputs to be used at any one speed without the liquid pool dropping through the sheet. The effect of ground position and electrode orientation on pool shape[8] were avoided by always having the electrode vertical and the ground attached to the rear of the pool. Current and voltage measurements were taken across the arc in

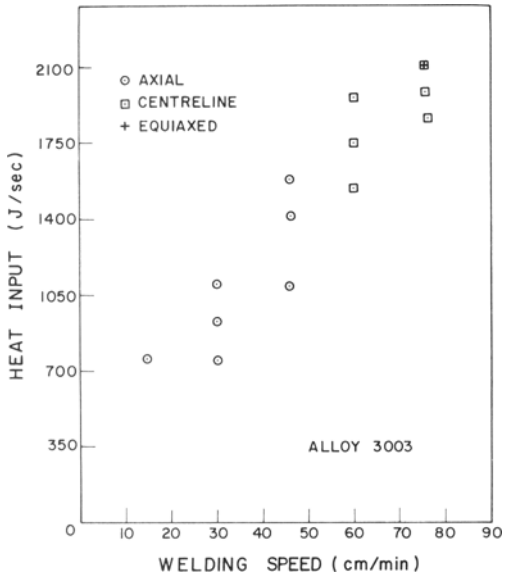

Fig. 2—Grain structures in alloy 3003 as a function of welding conditions.

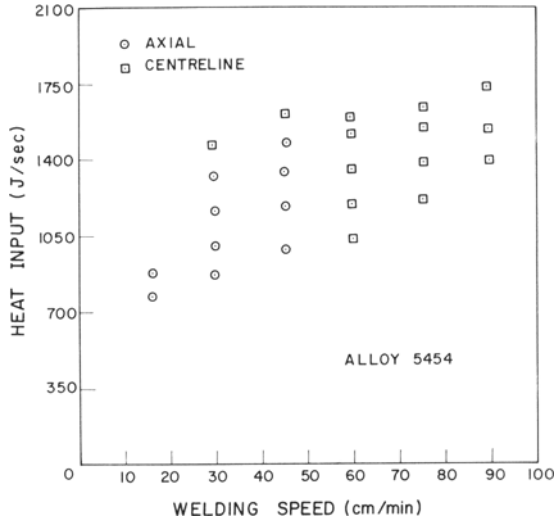

Fig. 3—Grain structures in alloy 5454 as a function of welding conditions.

Table II. Electropolishing Solutions and Conditions

Solution	Conditions	Alloy
475 ml methanol	stainless steel cathode	5083
8 ml nitric acid	14–20 V	7004
21 ml perchloric acid	0.8–1.2 A/cm²	
	18–21 °C	
400 ml ethanol	stainless steel cathode	all
24 ml perchloric acid	30–32 V	
	0.4–0.6 A/cm²	
	18–24 °C	
200 ml phosphoric acid	lead cathode	all
150 ml sulfuric acid	12–14 V	
275 ml water	2.7–3.5 A/cm²	
25 gm chromic oxide	80–85 °C	
250 ml phosphoric acid	lead cathode	
150 ml sulfuric acid	10–20 V	
200 ml water	0.6–0.8 A/cm² at	65–70 °C 1100
	2.2–2.7 A/cm² at	85–90 °C 7004

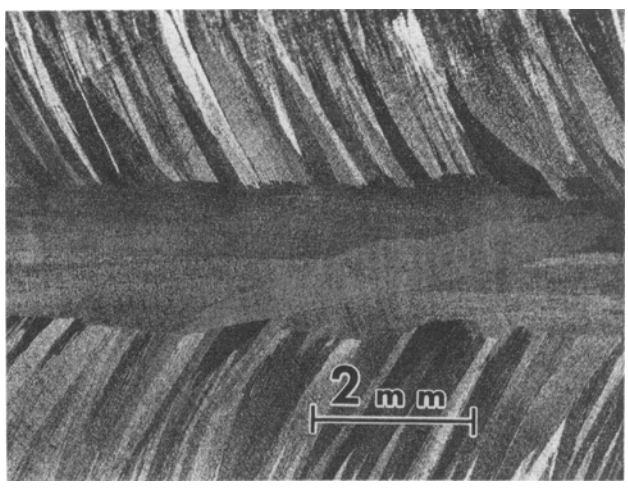

Fig. 4—Axial structure in alloy 3003 welded at 30 cm/min, 1090 J/s.

order to calculate the heat input per second.

Specimens were macroetched to reveal the overall grain structure using a solution containing 6 pct HF, 26 pct HNO_3 and 78 pct HCl. Electropolishing was carried out for microexamination at higher magnification using the solutions and conditions listed in Table II. The perchloric acid electrolytes produced a shiny surface in which the microsegregation pattern could be observed, but left pits at locations where second phases had existed. The electrolytes containing mixtures of sulfuric, phosphoric and chromic acids left such phases intact, allowing analysis of the small phases via the X-ray dispersive analyzer on the scanning electron microscope.

RESULTS

Grain Structures

Alloys 3003 and 5454. The terminology for various grain structures is the same as that employed for steel welds.[4] The summaries of the resulting structures in alloys 3003 and 5454 are shown in Figs. 2 and 3 respectively. Both alloys exhibited the axial grain structure (continuous grains in the welding direction at the weld center—Fig. 4) at the lower welding speeds and heat inputs, and the centerline structure (growth from the fusion boundaries to a distinct centerline—Fig. 5) at higher heat inputs and welding speeds. Although occasional new grains could be observed along the axial structure, as illustrated in Fig. 4, most of the axial grains initiated in the original weld bead and continued along the length of the weld.

With increasing weld speed the width of the axial region decreased and eventually disappeared, leaving the centerline structure. Pool shapes were revealed by emptying the molten pool with a gas jet. They showed that the decreasing width of the axial region with increased welding speed was due to the gradual change from an elliptical to a teardrop shaped pool limiting the region over which growth could take place parallel to the welding direction.

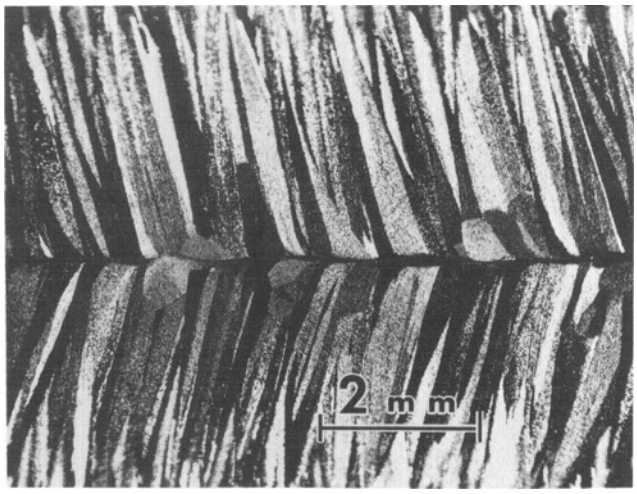

Fig. 5—Centerline structure in alloy 3003 welded at 60 cm/min, 1900 J/s.

In the centerline structure occasional large equiaxed grains could be seen near the weld center (Fig. 5). At the highest speed and heat input in alloy 3003 these were numerous enough to form an almost continuous region, as indicated in Fig. 2.

Alloys 1100, 5052 and 6061. The grain structures seen in these three alloys are summarized in Figs. 6 to 8. In all three alloys the stray structure was observed at low welding speeds and heat inputs. In this structure the dendrite orientations established near the fusion boundaries are replaced by different dendrite orientations closer to the centerline, as illustrated in Fig. 9. Unlike the axial structure, in the stray structure there is a continual appearance of new grains along the central region of the weld. But since many of these grains grow a considerable distance before they are restricted by the appearance of a new grain, they are not equiaxed. Thus the stray structure resembles the axial structure in that

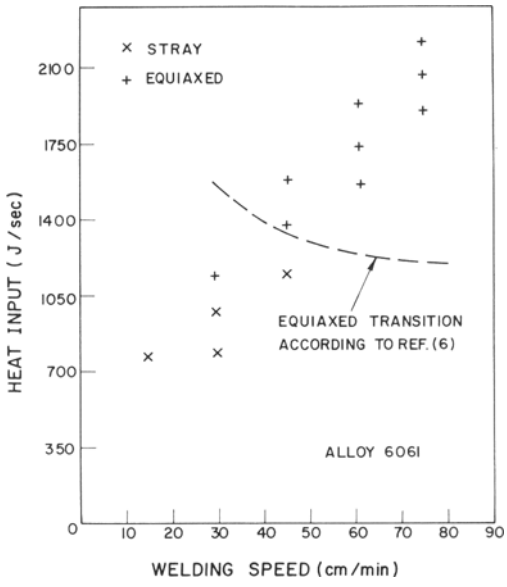

Fig. 6—Grain structures in alloy 6061 as a function of welding conditions.

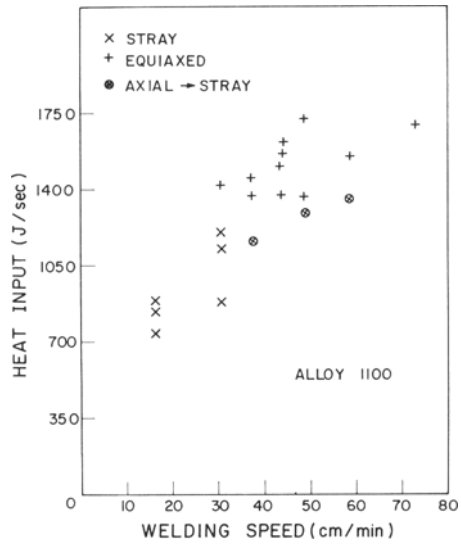

Fig. 7—Grain structures in alloy 1100 as a function of welding conditions.

grains tend to be oriented along the welding direction at the centerline, but in the stray structure each grain has a finite length which is less than the length of the weld. In alloy 1100, as noted on Fig. 7, a few welds began as axial structures but after some distance the appearance of new grains led to the stray structure.

At higher welding speeds and heat inputs these three alloys exhibited the equiaxed structure (Fig. 10); a band of equiaxed grains at the central region of the weld with columnar regions closer to the fusion boundaries. In alloy 5052 this central equiaxed region was often very narrow, so that Fig. 8 shows mixtures of centerline and equiaxed structures for these specimens. Hence the transition from the centerline to the equiaxed structure, like the axial/stray transition, is dependent on the frequency of the appearance of new grains. Figures 7 and 8 show that this transition is favored by increased heat input at a given weld speed.

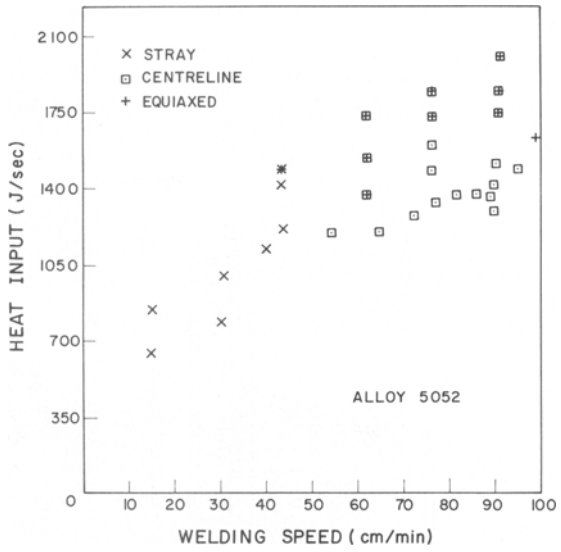

Fig. 8—Grain structures in alloy 5052 as a function of welding conditions.

Alloy 5083. This alloy exhibited an equiaxed structure at all weld speeds (Fig. 11). The width of the equiaxed zone was greater than illustrated for alloy 6061 in Fig. 10, ranging from 60 to 100 pct of the weld width, with equiaxed fraction increasing with heat input at a given welding speed. Arata *et al*[6] have also examined welds of this alloy, and found feathery grains or "completely columnar" grains to the left of the dotted line shown on Fig. 11, and equiaxed structures to the right.

Alloy 7004. The grain structures found in alloy 7004 are shown in Fig. 12. As in several other alloys, this alloy had an equiaxed structure at the highest heat inputs and welding speeds, but stray grains at the lowest welding speeds. At intermediate speeds and heat inputs, however, feathery grains were found along the center of the weld bead (Fig. 13).

Regression Analyses

The effect of an individual element on constitutional undercooling is predicted to be dependent on its effect on the freezing range, given by $mCo(1 - k)/k$, where m is the liquidus slope, k the distribution coefficient, and Co the percentage of the individual element. Commercial alloys contain many elements, making the use of m and k from binary aluminum alloys questionable. It is expected, however, that elements which show only limited solubility and hence have low values of k in

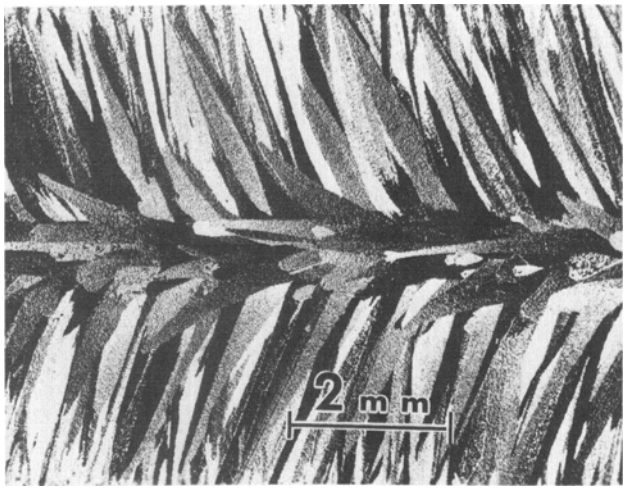

Fig. 9—Stray structure in alloy 5052 welded at 45 cm/min, 1440 J/s.

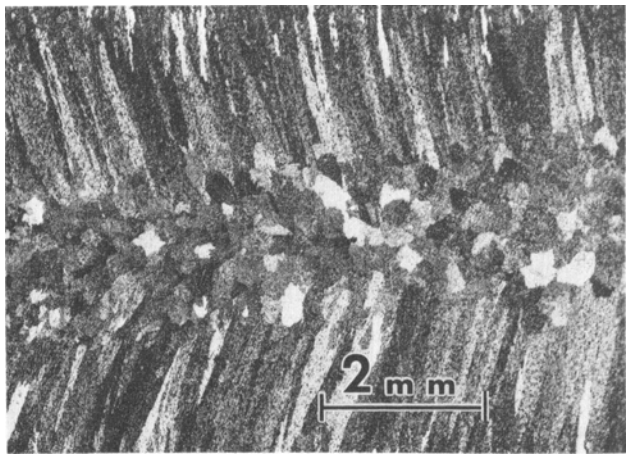

Fig. 10—Equiaxed structure in alloy 6061 welded at 75 cm/min, 1900 J/s.

Table III. Estimates of Parameter $m(1 - k)/k$ for Individual Elements from Binary Data

Element	Cu	Si	Fe	Mg	Mn	Zn	Cr	Ti
$m(1 - k)/k$	−16.6	−40.5	−90.5	−12.2	−0.21	−1.83	−1.04	−29.1

m = slope of liquidus line on binary Al-X phase diagram
k = estimated distribution coefficient for X in Al

binary alloys, will also have low values of k in the more complex alloys, making a substantial contribution to constitutional undercooling. Thus it was expected that the constants derived in a regression analysis of the tendency to form new grains *vs* composition might correlate with $m(1 - k)/k$ from binary alloys, if the hypothesis about the importance of the constitutional undercooling was correct. Values of $m(1 - k/k)$ for various solutes are given in Table III, using published binary phase diagrams.

To estimate the tendency of an alloy to form equiaxed grains, it was noted that the welding speeds employed ranged from 15 to 90 cm/min. These were used as boundary conditions for the "probability" of equiaxed grain formation, *i.e.*, 100 pct if the structure was equiaxed at 15 cm/min (*e.g.* alloy 5083—Fig. 11) and 0 pct if no equiaxed grains were observed (*e.g.* alloy 5454—Fig. 3). Linear interpolations at intermediate welding speeds along an "average" line for the welding conditions were employed for intermediate probabilities, as shown on Fig. 12. This method of assessing the tendency to form equiaxed grains led to the probabilities shown in Table IV for the present and previous[6] results. These probabilities were employed in a regression analysis *vs* weight percent of the major elements (Cu, Si, Fe, Mg, Mn, Zn, Ti). The resulting equation for the probability of finding equiaxed grains was:

$$\text{Pe(pct)} = -24.6 + 2067\ \text{Ti} + 13.9\ \text{Mg} + 53.7\ \text{Si} + 7.2\ \text{Cu} \quad [1]$$

Other elements did not have statistically significant effects.

In Eq. [1] the largest coefficient is for titanium, although Table III shows that titanium was not predicted to have the largest effect on constitutional undercooling.

At the lowest heat inputs and welding speeds the grain structures were either stray or axial. Alloy 5083 was equiaxed even at these conditions; this was taken as a fine-grain "stray" structure in the probability of stray grains shown in Table IV. A regression analysis for the probability of finding stray grains for these conditions

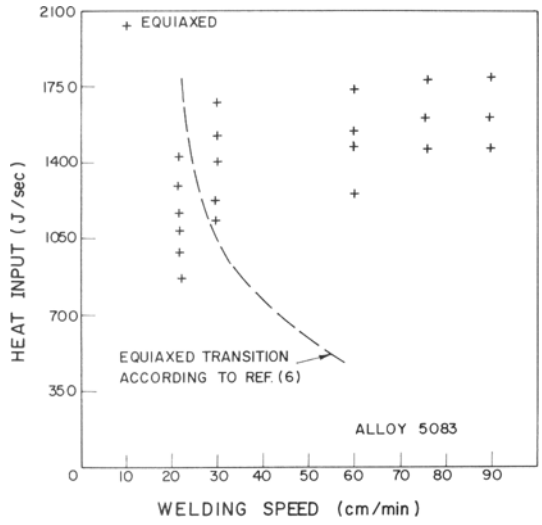

Fig. 11—Grain structures in alloy 5083 as a function of welding conditions.

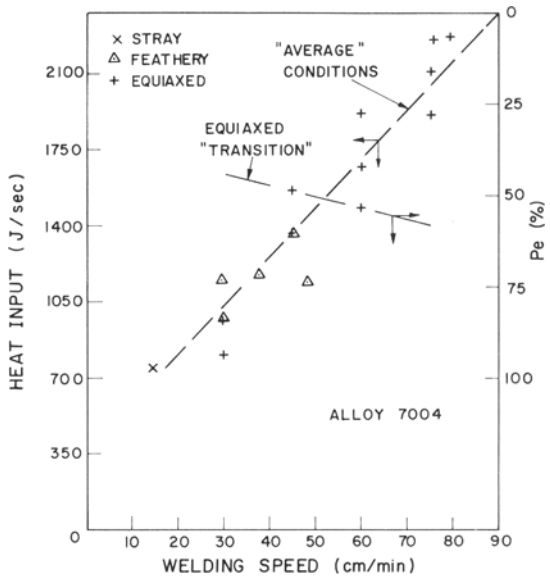

Fig. 12—Grain structures in alloy 7004 as a function of welding conditions.

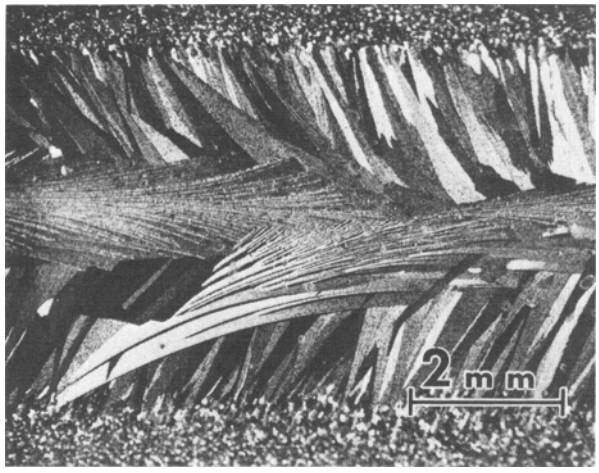

Fig. 13—Feathery grains along the centerline of alloy 7004 weld.

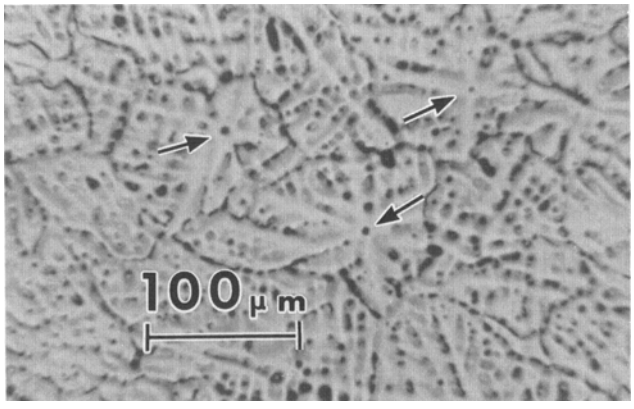

Fig. 14—Equiaxed grains in alloy 6061, showing pits at the centers of 3 dendrites (arrows).

was also carried out. In this case the resulting equation was:

$$Ps(pct) = 4476\ Ti \quad [2]$$

No other alloying elements had a statistically significant effect.

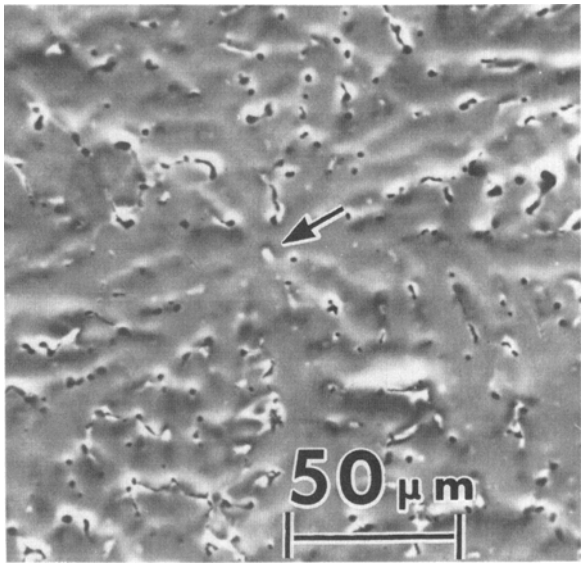

Fig. 15—Titanium-rich particle (arrow) at the center of a dendrite in alloy 7004.

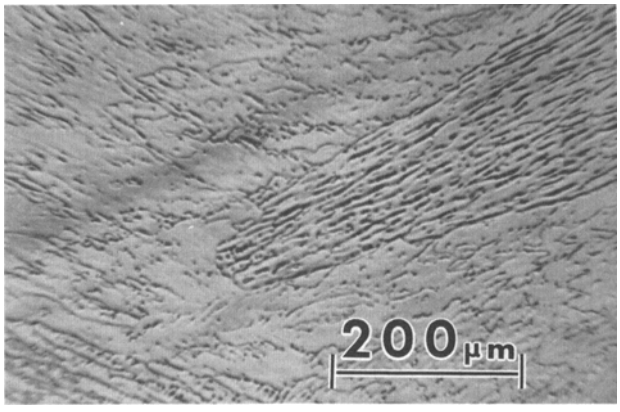

(a)

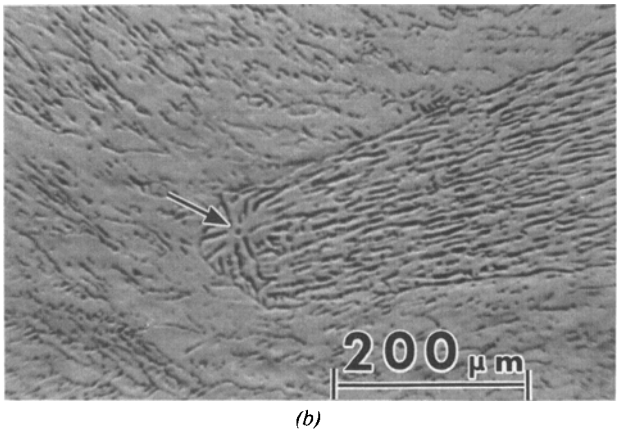

(b)

Fig. 16—Stray grain in alloy 3003 (*a*) above dendrite center, (*b*) through dendrite center, showing pit (arrow).

Hence in comparing stray *vs* axial structures, as well as the transition to equiaxed grains, regression analyses indicated that titanium had the largest effect of all elements. Titanium is widely known to produce second phases which act as nucleating agents in aluminum.[9] This suggested that these transitions are due to heterogeneous nucleation rather than either constitutional undercooling or dendrite arm remelting.

Examination of Individual Grains

The perchloric acid solutions listed in Table II were employed to examine equiaxed and stray grains in different alloys. Pits were observed close to dendrite centers in several specimens, as illustrated in Fig. 14 for alloy 6061. Examination of these pits at higher magnification failed to reveal second phases. However, the use of the phosphoric acid solutions listed in Table II did reveal second phases at the centers of dendritic equiaxed grains in alloys 1100, 5083, 6061 and 7004. An example is shown for alloy 7004 in Fig. 15. Analyses on the energy dispersive analyzer showed that these particles were rich in titanium in alloys 1100, 5083 and 7004. In alloy 7004 other particles were rich in zirconium or in both zirconium and titanium. Calculations uncorrected for absorption indicated that these particles contained up to 57 wt pct Ti or 32 wt pct Zr.

Two types of "stray" grains have been identified by Japanese workers who examined the surfaces of welds: those originating as branched crystals and others originating as equiaxed dendrites. In any one section both types may be observed, but only a few appear to originate as equiaxed grains, while others appear to be the "branched" type (Fig. 16(*a*)). By polishing down in successive steps, however, it was shown that a branched grain also originates as an equiaxed dendrite from a second phase, as illustrated in Fig. 16(*b*).

DISCUSSION

The presence of titanium-rich compounds in the centers of Al-rich dendrites indicates that the Al-rich phase was nucleated by these compounds. Phases which were not at dendrite centers were also analyzed and were found to contain other elements; magnesium in 5083 alloys, magnesium and silicon in 6061 alloy, and magnesium and zinc in 7004 alloy, consistent with Al_2Mg, Mg_2Si and $MgZn_2$ respectively.

Table IV. Observed Probabilities of Finding Equiaxed and Stray Grains

	Present Work		From Ref. 6	
Alloy	Probability (Pct)		Alloy	Probability (Pct)
	Pe	Ps		Pe	Ps
1100	37	100	1050	7	100
5052	20	100	2024	53	100
5083	100	100	3003	0	0
5454	0	0	5083	88	100
3003	0	0	6061	47	100
6061	60	100			
7004	50	100			

In a previous investigation of nucleation in Al-Ti alloys[9] several compounds, including TiC and Al_xTi, were identified as nucleants. The present analyses gave estimates (uncorrected for absorption) of up to 57 wt pct Ti. Since the beam is likely to have excited part of the surrounding Al-rich matrix, the actual nucleating particles were probably even richer in titanium. Hence it appears that Al_3Ti (37.3 wt pct Ti) was not the nucleating agent. TiC (80 to 90 wt pct Ti) could be the nucleating agent, not only because it has a high enough titanium content, but also because TiC is known to produce only one grain of aluminum per TiC particle,[10] as observed here. Another potential nucleant, TiB_2, also has a high titanium percentage (69 wt pct) but appears to nucleate Al_3Ti first rather than Al directly.[11] No evidence of this double nucleation step was found. Our energy analyzer cannot detect C or B X-rays, so that the compound(s) could not be positively identified.

The presence of zirconium in nucleating particles in alloy 7004 was at first surprising. This element was not reported in the original chemical analysis of the alloy, but it was confirmed on reanalysis (Table I). Another study[12] has shown that low concentrations of Zr aid grain refinement in Al alloys. The present finding that some particles contained both Zr and Ti suggests that a range of ternary compounds, possible Ti_xZr_yC, may act as nucleating agents for aluminum.

Although the results indicate that heterogeneous nucleation is the major mechanism of grain refinement, constitutional undercooling may play a role. The regression analysis for equiaxed grain formation (Eq. [1]) indicated that magnesium, silicon and copper had significant effects, in addition to titanium. Table III shows that, after iron, these three elements are predicted to have the most significant effects on constitutional undercooling. The range of iron contents in the alloys was small, making it difficult to determine its influence. Comparison of alloys with a given titanium content also shows the influence of other elements. For example Table IV shows that both 5052 and 3003 alloys contained 0.013 wt pct Ti, yet the former exhibited more equiaxed and stray grains (Fig. 4 *vs* Fig. 3).

In retrospect, once we were able to locate and partially analyze nucleating particles at the centers of dendrites, the results of the regression analyses were partly redundant. They are included for three reasons. First, the regression analyses originally showed the importance of titanium, and indicated the need for closer metallographic study. Other ways could be devised for defining "equiaxed probability", Pe, and "stray probability", Ps, and would result in different coefficients in Eqs. [1] and [2]. The importance of titanium was apparent first from the regression analysis, however, and was confirmed by the later metallographic study. Secondly, the regression analyses link both the stray and equiaxed structures to titanium, and hence to nucleation. Finally, the possible secondary influence of constitutional undercooling is underlined by the statistical study, as discussed above.

Arata *et al*[6] have observed that stray crystals appear to originate at a critical deviation of the dendrite axes from the direction of the maximum temperature gradient. The present results, especially Eq. [2], indicate that these grains originate by heterogeneous nucleation, rather than constitutional undercooling or breaking of dendrite arms. The survival, via growth, of a new grain depends on its growth temperature. When the dendrite axis is parallel to the maximum temperature gradient, then the macroscopic growth rate R and the growth rate parallel to the dendrite axis, Rd, are equal. If the dendrite axis deviates from the direction of the maximum temperature gradient by an angle θ, then $Rd = R/\cos\theta$. A larger undercooling is required to achieve $Rd > R$.[13] This permits a larger distance in front of the columnar grain in which a new grain can nucleate and grow before it is caught up in the macroscopic solid-liquid interface, so that the new grain will grow larger. If the dendrite axis of the new grain more closely parallels the maximum temperature gradient then the new grain will grow ahead of the original grain and thus survive.

In a given alloy, the percentage of stray or equiaxed grains depended on the welding conditions. In order for heterogeneous nucleation to change the grain structure, the new grains must grow large enough that they are not engulfed by the advancing interface. At a given macroscopic solidification velocity R, the temperature gradient G will determine the distance ahead of the macroscopic interface in which nucleation can occur. With a lower temperature gradient, nucleation can occur further ahead of the columnar interface, so that the new grains can grow larger before the columnar grains catch up to them. The temperature gradient decreases from the fusion boundary towards the centerline,[7] so that equiaxed grain formation is favored closer to the weld centers, as observed.

The temperature gradient along the weld centerline of a two dimensional weld is often estimated as

$$G_c = 2\pi\lambda\rho c\left(\frac{h}{Q}\right)^2 VT^3 \qquad [3]$$

where

λ = thermal conductivity
ρ = density
c = heat capacity
h = sheet thickness
Q = heat input per unit time
V = welding speed
T = the temperature difference between the melting temperature and the ambient temperature

At a given welding speed, V, the temperature gradient predicted by Eq. [3] decreases as the heat input is increased. This is consistent with the observation that increasing the heat input at a given weld speed led to equiaxed structures, when sufficient titanium or zirconium was present (Figs. 7 and 8).

At a given heat input, increased welding speed, V, also tends to cause equiaxed grains, according to Ref. 6. This appears inconsistent with casting experiments in which faster solidification resulted in fewer equiaxed grains by heterogeneous nucleation.[14] At faster solidification rates individual grains ahead of the columnar interface have less time to grow large enough to block columnar growth. Equation [3] shows that Gc increases

as V is increased, which also suggests that columnar rather than equiaxed grains should result, as discussed above. According to Eq. [3] the ratio Gc/V remains constant with increased welding speed, so that constitutional undercooling effects are also approximately constant. The ratio G/R (local temperature gradient over local solidification velocity) depends on the angle ϕ between the welding direction and the solid-liquid interface.[4] Although this angle decreases if both heat input and speed are increased, the effect of increased welding speed alone is predicted to be to decrease the pool size without changing its shape.[15] Hence G/R is also predicted to remain constant with increased weld speed.

Increased solidification velocity also increases the growth undercooling. For dendrites the growth undercooling is approximately proportional to the square root of the solidification velocity.[13] This will tend to increase the time available for nuclei to grow, but is offset by the effects of the welding speed on G and R (Appendix I).

The most likely explanation of the effect of velocity at a given heat input is that fewer nucleating particles are melted or dissolved at the higher welding speeds, allowing a higher nucleation frequency. This conclusion also appears to be consistent with studies of the effects of fluid flow on equiaxed grain formation which are presently in progress.

The feathery structure observed elsewhere[6] in 5083 at low welding speeds was not observed in our specimens of this alloy, presumably because the titanium content in our alloy was slightly higher, causing equiaxed grains at all conditions. We did observe feathery grains in 7004 alloy, (Fig. 13) caused by twin growth. It is clear that increased nucleation frequency avoids feathery growth, and some of its inherent problems.

SUMMARY

The grain structures of two dimensional GTA welds have been studied in sheets of a number of commercial aluminum alloys; 1100, 3003, 5052, 5454, 6061 and 7004. At low welding speeds and heat input either axial grains along the weld centerline or large elongated "stray" grains were observed, with columnar grains closer to the fusion boundaries. At high welding speeds the columnar grains either grew all the way to the centerline or were blocked by equiaxed grains.

Both the axial to stray and the centerline to equiaxed transitions were strongly favored by titanium, consistent with the observation of titanium-rich compounds in the centers of equiaxed dendrites in several alloys. In 7004 alloy both zirconium and zirconium-titanium rich compounds were observed at dendrite centers.

It is concluded that both equiaxed and stray grains originate by heterogeneous nucleation, possibly by Ti_xZr_yC compounds, aided by constitutional undercooling.

Increased heat input aids the formation of equiaxed grains by allowing more time for nucleus growth due to a decreased temperature gradient. Increased welding speed appears to favor the heterogeneous nucleation process by allowing less time for melting of the potential nuclei.

APPENDIX I

The growth of new grains of aluminum takes place betwen the equilibrium freezing temperature of the alloy Tm, and the growth temperature of the columnar grains T_G. For dendritic growth, this undercooling is approximately given by[13]

$$\Delta T = A R^{1/2} \qquad [1a]$$

where A is a constant for a given material. For a linear temperature gradient G ahead of the interface, this undercooling corresponds to a distance $\Delta X = \Delta T/G$ which for an interface advancing at velocity R corresponds to a time

$$\Delta t = \frac{\Delta T}{GR} \qquad [2a]$$

Close to the weld centerline for a tear-drop shaped pool, if ϕ is the angle between the macroscopic solid-liquid interface and the welding direction, then $G = G_c/\sin\phi$ and $R = V \sin\phi$ where G_c is the temperature gradient along the centerline and V the welding speed. According to Eq. [3], for a fixed heat input Q,

$$G_c = BV \qquad [3a]$$

where B is a constant for a given material. Substituting into Eq. [2a]

$$\Delta t = \frac{\Delta T}{BV^2}$$

$$= \frac{A}{B} V^{-3/2} (\sin\phi)^{1/2}$$

Hence the time for growth of nuclei ahead of the macroscopic interface decreases as the welding speed increases.

ACKNOWLEDGMENTS

The aluminum alloy sheet and chemical analysis were graciously provided by the Aluminum Company of Canada. This work was supported financially by a grant from the National Research Council of Canada (now Natural Sciences and Engineering Research Council of Canada).

REFERENCES

1. W. F. Savage: *Weldments: Physical Metallurgy and Failure Phenomena*, R. J. Christoffel *et al*, ed., General Electric Co., Schenectady, NY, 1979, pp. 1–18.
2. J. Hernaez and A. Madronero: *Weld. J.*, 1972, vol. 51, pp. 281-S–294-S.
3. G. J. Davies and J. G. Garland: *Int. Metall. Rev.*, 1975, vol. 20, pp. 83–106.
4. T. Ganaha and H. W. Kerr: *Met. Technol.*, 1978, vol. 5, pp. 62–69.
5. M. Kato, F. Matsuda and T. Senda: *Weld. Res. Abroad*, 1973, vol. 19(2), pp. 26–33.
6. Y. Arata, F. Matsuda, and A. Matsui: *Trans. Jpn. Weld. Res. Inst.*, 1974, vol. 3, pp. 89–97.
7. H. W. Ghent, C. E. Hermance, H. W. Kerr, and A. B. Strong: *Arc Physics and Weld Pool Behaviour*, Conference Proceedings, The Welding Institute, Cambridge, UK, 1979.

8. W. H. S. Lawson and H. W. Kerr: *Weld. Res. Int.*, 1976, vol. 6(5) pp. 63–77 and 6(6), pp. 1–17.
9. J. Cissé, H. W. Kerr and G. F. Bolling: *Met. Trans.*, 1974, vol. 5, pp. 633–641.
10. J. Cissé, G. F. Bolling and H. W. Kerr: *J. Cryst. Growth*, 1972, vol. 13/14, pp. 777–81.
11. A. J. Cornish: *Met. Sci.*, 1975, vol. 9, pp. 477–484.
12. G. W. Delamore and R. W. Smith: *Met. Trans.*, 1971, vol. 2, pp. 1733–38.
13. B. Chalmers: *Principles of Solidification*, J. Wiley and Sons, New York, 1964, p. 106.
14. G. F. Bolling: *Solidification*, ASM, Metals Park, OH, 1971, p. 365.
15. J. F. Lancaster: *The Metallurgy of Welding, Brazing and Soldering*, Geo. Allen and Unwin, London, 1970, p. 48.